Title

Large-pore connexin hemichannels function like molecule transporters independent of ion conduction

Journal

Proceedings of the National Academy of Sciences of the United States of America, 121(33)

ISSN

0027-8424

Authors

Gaete, Pablo S

Kumar, Deepak

Fernandez, Cynthia I

et al.

Publication Date

2024-08-13

DOI

10.1073/pnas.2403903121

Peer reviewed

PNAS RESEARCH ARTICLE | PHYSIOLOGY OPEN ACCESS

Large-pore connexin hemichannels function like molecule transporters independent of ion conduction

Pablo S. Gaete[a], Deepak Kumar[b], Cynthia I. Fernandez[a], Juan M. Valdez Capuccino[c], Aashish Bhatt[b], Wenjuan Jiang[b], Yi-Chun Lin[b], Yu Liu[c], Andrew L. Harris[c], Yun L. Luo[b], and Jorge E. Contreras[a,1]

Affiliations are included on p. 11.

Edited by Juan Saez, Universidad de Valparaiso, Valparaiso, Chile; received March 14, 2024; accepted July 5, 2024

Connexin hemichannels were identified as the first members of the eukaryotic large-pore channel family that mediate permeation of both atomic ions and small molecules between the intracellular and extracellular environments. The conventional view is that their pore is a large passive conduit through which both ions and molecules diffuse in a similar manner. In stark contrast to this notion, we demonstrate that the permeation of ions and of molecules in connexin hemichannels can be uncoupled and differentially regulated. We find that human connexin mutations that produce pathologies and were previously thought to be loss-of-function mutations due to the lack of ionic currents are still capable of mediating the passive transport of molecules with kinetics close to those of wild-type channels. This molecular transport displays saturability in the micromolar range, selectivity, and competitive inhibition, properties that are tuned by specific interactions between the permeating molecules and the N-terminal domain that lies within the pore—a general feature of large-pore channels. We propose that connexin hemichannels and, likely, other large-pore channels, are hybrid channel/transporter-like proteins that might switch between these two modes to promote selective ion conduction or autocrine/paracrine molecular signaling in health and disease processes.

molecular transport | permeation | selectivity | gap junction channel

Connexin proteins assemble as hexamers to form hemichannels that are inserted in the plasma membrane. The docking of two hemichannels in apposed cells forms a gap junction channel (GJC) that allows direct cytoplasmic communication. Connexin hemichannels were the first identified plasma membrane channels with unique properties that mediate both the flux of atomic ions and the permeation of small molecules like ATP and glutamate. Opening of undocked hemichannels has been extensively associated with numerous pathological outcomes, which suggested that in physiological conditions these hemichannels remain mainly silent (i.e., in a closed state) to maintain the cellular electrochemical gradient. Nevertheless, a critical role for undocked hemichannels in physiological processes via the release of cytosolic molecules mediating autocrine and paracrine roles has emerged (1–5). How ion fluxes and molecular permeation coexist to mediate both physiological and pathological outcomes is still unclear.

Structural studies have revealed that connexin hemichannels have a wide pore cavity, with all six highly flexible N-terminal (NT) domains lining the pore in the cytosolic entrance and forming the narrowest part of the conduction pathway (6–11). Although a fully physiological closed state has not been clearly captured yet, some of the resolved structures revealed a conformation with a pore entrance that was narrowed to a diameter of ~5 to 8 Å, which could reflect a conformation in which only ions but not molecules can permeate (9–11). Functional assays showing the permeation of different small molecules suggested that the fully open hemichannel conformation for permeation of molecules has an estimated limiting diameter of around ~12 to 15 Å (5), which is likewise wide enough to allow ion fluxes. This has been partially supported by some structural studies (6–8); however, the mechanisms involved in molecular transport through the pore are still largely unknown. The present understanding is that molecular permeation in connexin hemichannels should be well-correlated with the movement of atomic ions, subject to size constraints, as suggested earlier for GJCs (12, 13). Under this rationale, the flux of both atomic ions and molecular permeants should proportionally increase, since a large pore size would act as a major determinant for both ion conductance and molecule permeation.

This notion, however, is inconsistent with findings showing uptake of fluorescent small molecules through connexin hemichannels (and the large-pore channels formed by pannexins) when there are negligible or undetected ionic currents, in particular at resting membrane potentials (14–19). Furthermore, pharmacological blockade of connexins or pannexins has been shown to differentially affect atomic ion and molecule permeation

Significance

The mechanism behind molecule permeation through large-pore connexin hemichannels remains enigmatic. The current perspective posits that ions and molecules diffuse simultaneously, with molecule selectivity and permeability mainly relying on pore size constraints. Our study challenges this view by demonstrating that molecules permeate hemichannels via mechanisms akin to transporters or carriers. We find that molecule transport is uncoupled from ion flux, suggesting distinct conformational states for molecule and ion conduction. These findings redefine our understanding of connexin hemichannel function, indicating roles beyond a simple conduction pathway and highlighting implications for health and disease. Our work underscores the need to reassess the mechanisms of molecule and ion flux in other large-pore channels.

Author contributions: P.S.G., Y.L.L., and J.E.C. designed research; P.S.G., D.K., C.I.F., J.M.V.C., W.J., and Y.-C.L. performed research; A.B. and Y.L. contributed new reagents/analytic tools; P.S.G., D.K., C.I.F., and J.M.V.C. analyzed data; P.S.G. and Y.L. performed molecular biology; P.S.G., A.L.H., Y.L.L., and J.E.C. edited the manuscript; W.J. and Y.-C.L. prepared ethidium simulation system; Y.L.L. and J.E.C. oversaw research; and P.S.G., D.K., A.L.H., Y.L.L., and J.E.C. wrote the paper.

The authors declare no competing interest.

This article is a PNAS Direct Submission.

[1]To whom correspondence may be addressed. Email: jecontrer@ucdavis.edu.

This article contains supporting information online at https://www.pnas.org/lookup/suppl/doi:10.1073/pnas.2403903121/-/DCSupplemental.

Published August 8, 2024.

(15, 16). Given the importance of molecular signaling in physiology and pathology, the lack of understanding of this anomalous permeation phenomenon has been a confounder in understanding the biological and pathological roles of connexin hemichannels as well as for other large-pore channels.

To explore the mechanisms underlying the permeation of small molecules and ions in hemichannels, we evaluated the biophysical properties of permeation of two small fluorescent cationic dyes, ethidium and DAPI, whose permeation has been extensively used for assessing connexin hemichannel activity. By combining MD simulations, dye uptake assays, mutagenesis, cross-linking, and electrophysiology, we found that permeation of molecules through connexin hemichannels exhibits properties that include saturability, competitive inhibition, selectivity, and discrete binding sites for molecules within the pore, reminiscent of classical transporter properties. We demonstrate that while ions and molecules use the same permeation pathway, the transport of molecules can be uncoupled from ion fluxes. We propose that connexin hemichannels may adopt different pore conformations that allow NT rearrangements to work either as ion channel or transporter for molecules. This finding has profound implications for our understanding of how connexin hemichannels, and perhaps large-pore channels in general, function in health and disease.

Results

Transport of Molecules through Connexin Hemichannels Is Selective and Saturable. To properly understand how ions and molecules permeate through the connexin hemichannel pore, we recently developed a TEVC/dye uptake assay that measures kinetics of transport of fluorescent dyes and ionic current simultaneously in a single cell (19, 20). First, we compared the permeability of two membrane-impermeant fluorescent dyes, DAPI and ethidium, in two closely related connexin isoforms, Cx26 and Cx30 (85.4% sequence identity). In line with previous findings (19), we found that Cx26 hemichannels were permeable to DAPI but not to ethidium (Fig. 1 *A* and *B*), indicating a clear molecular selectivity. DAPI uptake through Cx26 hemichannels was concentration-dependent and saturated in the mid micromolar range (Fig. 1 *C* and *D*). In contrast, Cx30 hemichannels were permeable to ethidium but not to DAPI (Fig. 1 *E* and *F*). Ethidium permeation through Cx30 hemichannels saturated in the low micromolar range (Fig. 1 *G* and *H*). The Km values for transport of these molecules were connexin isoform-specific: 90.1 ± 22.0 μM for DAPI in Cx26 and 6.6 ± 2.0 μM for ethidium in Cx30. This indicates that molecular transport through these two hemichannels is highly selective due to specific interactions between the permeants and the connexin channel pores.

Interactions between Permeants and the NT Domain Determine Selectivity and Kinetics of Molecule Permeation. To gain insights into the mechanisms of molecule permeation through these hemichannels, we performed MD simulations. For this purpose, we used our equilibrated Cx26 hemichannel model, with which we have recapitulated experimental single-channel permeability of cAMP at ±200 mV and Markovian milestoning simulations without voltage (21–23). Here, we examined qualitatively both ethidium (+1e) and DAPI (+2e) inward transport at −200 mV through the Cx26 hemichannel to identify potential protein-permeant interactions that may be responsible for the differences in permeability observed experimentally.

Three replicas of 500 ns all-atom simulations revealed two major ethidium binding regions in the Cx26 pore, one at the extracellular end and one at the NT region (roughly z = +20 Å and −10 Å, respectively) (Fig. 2 *A* and *B*). The heightened probability density distribution in the extracellular region is attributed to electrostatic and van der Waals interactions with anionic side chain residues, including Glu42, Asp46, Glu47, and Asp50

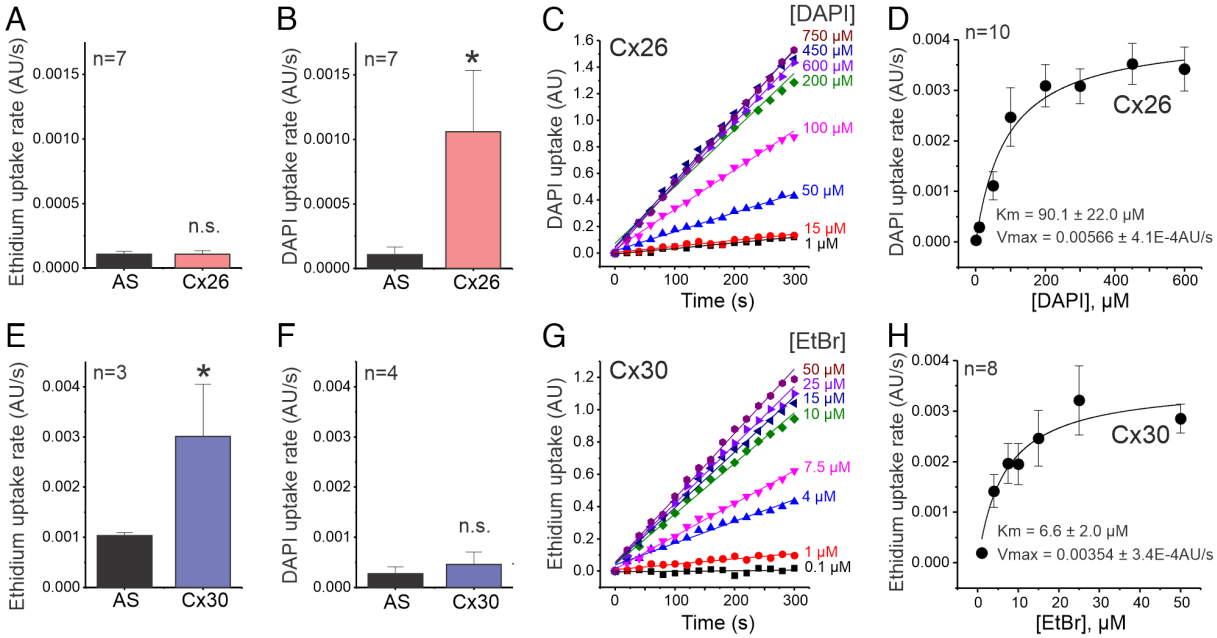

Fig. 1. Transport of molecules through connexin hemichannels is selective and saturable. Dye uptake was evaluated in *Xenopus* oocytes expressing Cx26 (*A*–*D*) or Cx30 (*E*–*H*) at resting membrane potentials. Oocytes injected with antisense alone (AS) were used as controls (*Materials and Methods*). (*A*) Ethidium uptake rate detected in oocytes incubated with 50 μM ethidium bromide (EtBr). (*B*) DAPI uptake rate detected in oocytes incubated with 50 μM DAPI dilactate. (*C*) Representative time courses of Cx26-mediated DAPI uptake. The concentration of DAPI dilactate in the extracellular bath is shown next to each trace. (*D*) Quantification of the DAPI uptake rate shown in *C*. (*E*) Ethidium uptake rate detected in oocytes incubated with 50 μM EtBr. (*F*) DAPI uptake rate detected in oocytes incubated with 50 μM DAPI dilactate. (*G*) Representative time courses of Cx30-mediated ethidium uptake. The concentration of ethidium bromide in the extracellular bath is shown next to each trace. (*H*) Quantification of the ethidium uptake rate shown in *G*. Data in *D* and *H* were fit with the Michaelis–Menten equation to calculate Km and Vmax. *$P < 0.05$ vs. AS by unpaired Student's *t* test. n.s.= nonsignificant. Error bars are SEM.

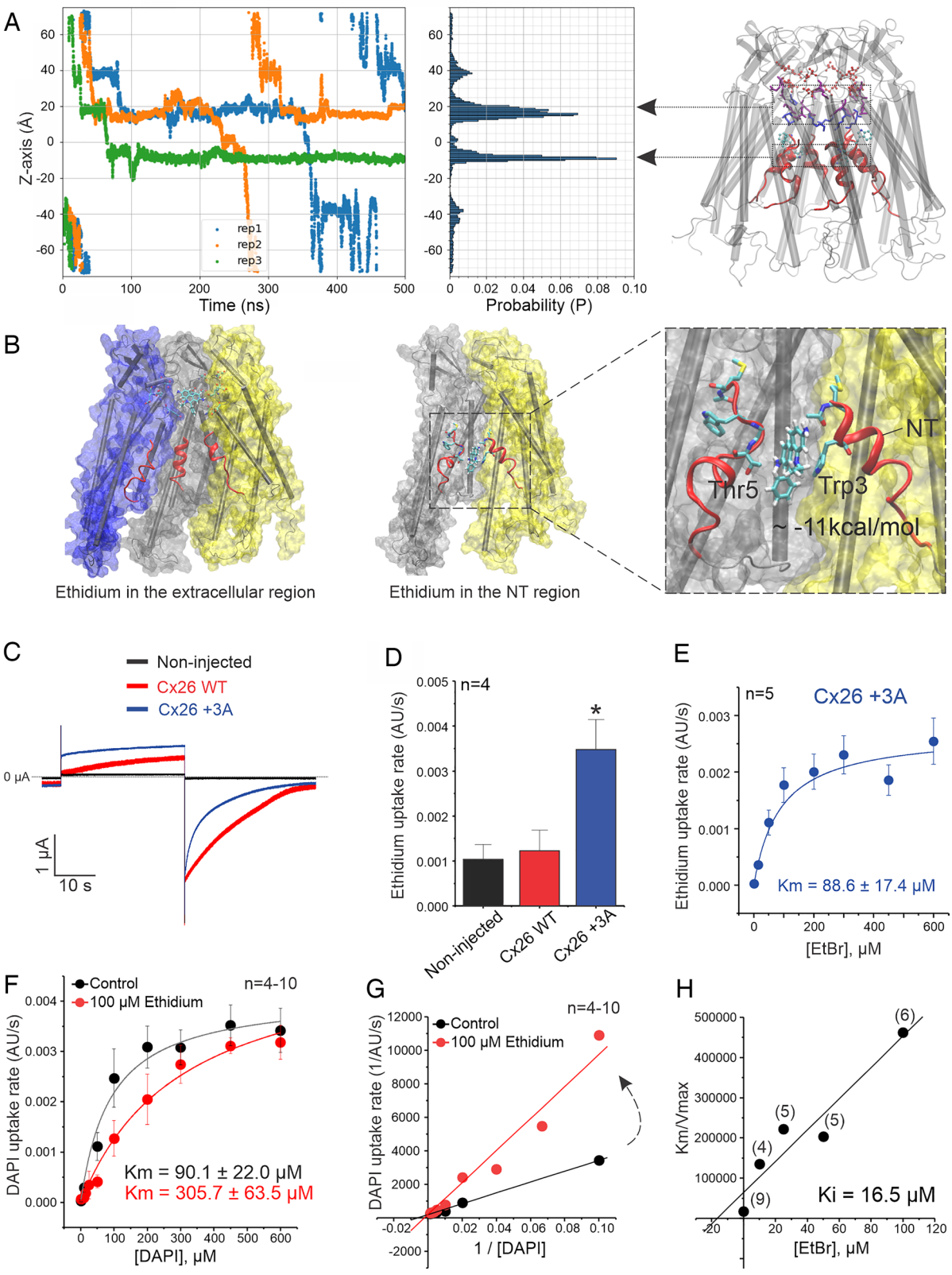

Fig. 2. The NT domain interacts with molecules and confers selectivity properties to connexin hemichannels. (*A*) MD simulations of ethidium permeation through Cx26 hemichannels. Traces represent the Z coordinates of the ethidium molecule. Flux is inward (from positive to negative Z coordinates) at −200 mV. Three independent replicas are shown in blue, orange, and green. The distribution probability analysis reveals two major interaction regions inside the pore. (*B*) Snapshot showing one ethidium molecule interacting in the extracellular region (*Left*) and when trapped in the NT domain (*Middle*). The total interaction energy for ethidium and Trp3 is shown (*Right*). (*C*) Representative ionic current traces from oocytes expressing Cx26 wild-type (WT) or the mutant Cx26 +3A. Noninjected oocytes were used as controls. (*D*) Ethidium uptake rate recorded in oocytes incubated with 50 µM ethidium bromide (EtBr). (*E*) Concentration–response curve for ethidium uptake in oocytes expressing the mutant Cx26 +3A. (*F*) Effect of a saturating ethidium concentration on DAPI permeation. Experiments were performed in oocytes expressing Cx26 WT. (*G*) Lineweaver–Burk plot obtained from data shown in *F* reflects the competitive inhibition of ethidium on DAPI permeation. (*H*) Calculation of the inhibition constant (Ki) for ethidium. The n values for each point in this figure are shown in parentheses. Data in *E* and *F* were fit with the Michaelis–Menten equation to calculate Km. Dye uptake was evaluated at resting membrane potentials. *$P < 0.05$ vs. noninjected, by one-way ANOVA plus Newman–Keuls post hoc test. Error bars are SEM.

(Fig. 2*B* and *SI Appendix*, Fig. S1). Within 500 ns, we observed complete permeation events in two of the replicates, suggesting that these interactions are short-lived (residence time 150 to 300 ns under −200 mV). In the NT region, however, ethidium exhibited a prolonged pi-stacking interaction with Trp3 sidechains in the third replica. This is consistent with our interaction analysis showing that the interaction between ethidium and Trp3 is the strongest among all pore-lining residues (*SI Appendix*, Fig. S1). We noticed that the relative orientation between ethidium and Trp3 sidechain plays a pivotal role in determining the access of ethidium through the Cx26 pore. The equatorial diameter of ethidium is 9.7 Å, smaller than the minimum pore diameter of 14 Å. Thus, ethidium can assume various orientations within the pore. When ethidium approaches the NT region of the pore horizontally, with its rings parallel to the membrane plane, the likelihood of establishing pi-stacking with Trp3 diminishes, while a vertical orientation of ethidium facilitates such interaction. When this interaction occurs, ethidium becomes trapped between Trp3 and the Thr5 from the neighboring subunit throughout the trajectory, presenting a basis for its impermeability (Fig. 2*B*).

Due to the limited sampling time and the stochastic nature of the nonequilibrium voltage simulations, the strong pi-stacking between ethidium and Trp3 was captured in only one replica. Hence, to experimentally verify whether this is indeed the dominant interaction that impairs the permeability of ethidium in Cx26 hemichannels, we performed site-directed mutagenesis with the rationale of decreasing the ethidium affinity at this putative binding site. First, we inserted an alanine at position 3, next to the Trp3 (Cx26 +3A). The mutant containing this insertion formed functional hemichannels with biophysical properties comparable to those of wild type, including similar gating properties, voltage dependence, and sensitivity to extracellular Ca^{2+} concentrations, indicating that atomic ion permeation and global regulatory properties remain largely unchanged (Fig. 2*C* and *SI Appendix*, Fig. S2). More importantly, the Cx26 +3A mutation enabled ethidium permeation (Fig. 2*D*). A concentration–response analysis revealed that the transport of ethidium through this mutant hemichannel was saturable with a Km = 88.6 ± 17.4 μM (Fig. 2*E*). This Km is similar to that of DAPI in WT Cx26, suggesting the binding affinity of ethidium in Cx26 +3A is in the same range as that of DAPI in WT Cx26. The data suggest that with the insertion of the Ala, Trp3 was either displaced deeper into the pore (further away from the Thr5 of the adjacent subunit) or reconfigured so that it could not form pi–pi interactions with ethidium. To distinguish these possibilities, Trp3 was substituted by alanine (W3A). This mutation also enabled ethidium permeation, and to the same degree as the Cx26 +3A, showing that indeed the interaction of ethidium with Trp3 is what renders Cx26 impermeable to ethidium. Unexpectedly, the W3A mutation, in addition to enabling ethidium permeation, eliminated ionic currents (*SI Appendix*, Fig. S3). This striking initial finding is explored further in later experiments.

If ethidium has access to the WT Cx26 hemichannel pore and remains trapped at the NT-lined pore region, as predicted by MD simulations and supported by experiments, then its presence in the pore should decrease DAPI permeation in a concentration-dependent manner, since DAPI must traverse the same region to permeate. Consistent with this, we found that the apparent affinity for DAPI is reduced in the presence of 100 μM ethidium (Fig. 2*F*). Interestingly, a Lineweaver–Burk plot indicated that ethidium acts as a competitive inhibitor for DAPI permeation (Fig. 2*G*). A Km/Vmax relationship was obtained for DAPI permeation in the presence of different ethidium concentrations to estimate the inhibition constant (Ki). The Ki value for DAPI transport inhibition by ethidium was ~16.5 μM (Fig. 2*H*). These data suggest that ethidium competes with or interferes with access to the DAPI binding site within the pore.

Voltage simulations were conducted to identify DAPI–pore interactions. DAPI (+2e) is a long and rigid molecule with +1e at each end. Its equatorial distance of 13.6 Å is comparable to the minimum pore diameter at the NT region. Although larger than ethidium, six permeation events were observed during three replicas of 500 ns DAPI simulations (Fig. 3*A*). In all replicas, DAPI established consistent interactions with Cx26 at several locations inside the pore (Fig. 3 *A* and *C*). At the extracellular entrance, DAPI lays horizontally and interacts with the Asp50 sidechain of one subunit, and Asp46 and Glu47 from the opposite subunit (Fig. 3 *B*, *Inset 1*). This is followed by breaking of the interaction with Asp50 to form a new interaction with Glu42 in the same subunit (Fig. 3 *B*, *Inset 2*). Next, DAPI breaks the interaction with Glu47 and Glu42 and forms new interactions with two Asp2 in the neighboring NT helices (Fig. 3 *B*, *Insets 3 and 4*). However, the DAPI–Asp2 interaction has shorter lifetime (<100 ns) than ethidium–Trp3 interaction (>400 ns). Breaking the charge–charge interaction with one of the Asp2 residues reorients DAPI vertically in the pore, which allows DAPI to pass through the narrowest pore region (*SI Appendix*, Fig. S4).

To confirm DAPI's interaction with Asp2 at the NT domain, we replaced residue Asp2 with asparagine (D2N). As expected, the D2N mutation was still permeable to DAPI, but it lowered the apparent affinity ~3-fold without affecting the maximum transport velocity (Fig. 3*D*). Altogether, our in silico and functional data demonstrate that DAPI and ethidium interact with the NT domain through different types of interactions, selectivity and transport kinetics are determined by these interactions.

NT Domain Rearrangements Are Necessary for the Permeation of Molecules. Structural studies show that the narrowest pore region in Cx26 hemichannels is located in the NT domain, where DAPI and ethidium interact. Therefore, we asked whether the dynamics of NT domain are coupled with molecular permeation. In all three replicas of 500 ns simulations, DAPI interaction with a single NT domain led to a slight unfolding of the interacting NT and pulled it toward the cytoplasmic entrance, reflected in the distance between Met1 of adjacent subunits (*SI Appendix*, Fig. S5). This rearrangement was coupled with a loss of interactions between the NT domain and the TM1 helix, including a salt bridge between Asp2 and Lys41, and hydrophobic interactions between Trp3-Met34 and Trp3-Ile33 (*SI Appendix*, Fig. S6). These observations suggest that permeation of DAPI through the pore exerts effects on the conformational dynamics of the NT.

To assess whether conformational rearrangements of the NT are necessary for permeation of molecules, we created a mutant channel with a cysteine inserted in the NT domain at position 2 (named Cx26B +2C, Fig. 4*A*, and *SI Appendix*, Fig. S7). In this mutant, residues C211 and C218 were replaced with serine to prevent unspecific effects. Thus, hemichannels including C211S and C218S but not the cysteine at position 2 (named Cx26B) were used as control. We then assessed the rate of disulfide bridge formation between adjacent cysteines in a state-dependent manner in the presence of an oxidant agent, $TBHO_2$. For this, we used the well-known ability of millimolar extracellular Ca^{2+} to induce a closed state of connexin hemichannels (24). First, we showed that the Cx26B +2C mutant hemichannels displayed similar Ca^{2+}-gating sensitivity when compared to WT hemichannels (*SI Appendix*, Fig. S7). Fig. 4*B* shows representative ionic current traces for Cx26B and Cx26B

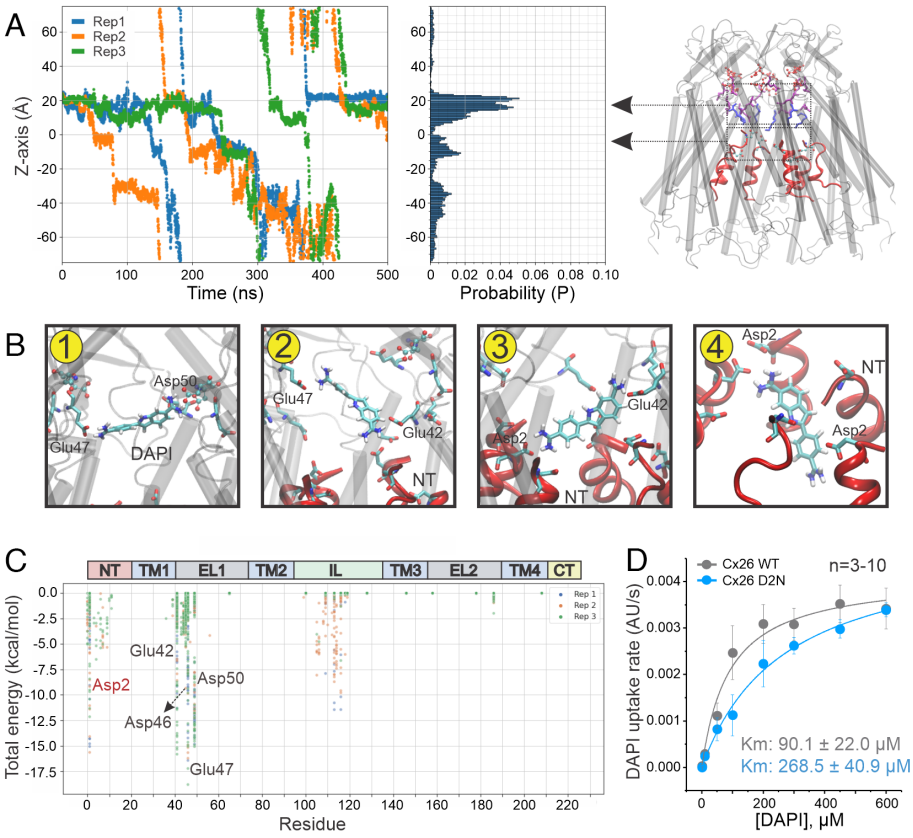

Fig. 3. Interactions between permeants and the NT domain determine the kinetics of molecular permeation. (*A*) Simulations of DAPI permeation through Cx26 hemichannels. Traces represent the Z coordinates of the DAPI molecule when the flux is inward (under −200 mV). Three independent replicas are shown in blue, orange, and green. A snapshot of the simulated system is shown in the *Right* panel. The protein backbone is shown using gray cylindrical helices in cartoon mode. NT domains are highlighted in red. (*B*) One DAPI molecule and the sidechains interacting with DAPI during a single permeation event are shown in licorice with atom color code (red, oxygen; cyan, carbon; blue, nitrogen; white, hydrogen). Lipids, ions, and water molecules are not shown for clarity. Panels 1 to 4 represent the interactions between DAPI and the residues lining the pore during the permeation process. *Inset 1*: DAPI interaction in the extracellular region of the pore; *Inset 2*: DAPI translocation to the NT region; *Inset 3*: DAPI interaction with the NT domain; *Inset 4*: DAPI translocation to the intracellular region (see *Results* for detailed description). Transmembrane domains are not shown in *Inset 4* for clarity. (*C*) An MMGB pairwise analysis was performed to calculate the total interaction energies between DAPI and the residues lining the pore of Cx26 hemichannels. (*D*) The effect of D2N mutation on DAPI permeation unveils the importance of the NT in the control of molecule permeation kinetics. DAPI uptake was evaluated at resting membrane potentials. Error bars are SEM.

+2C in the presence of 0.1 mM and 5 mM Ca^{2+}, two conditions that favor opening and closing of hemichannels, respectively. When 2 mM $TbHO_2$ was superfused to promote formation of disulfide bridges, a monoexponential decay of the ionic currents was observed in the Cx26B +2C but not in the Cx26B hemichannels, suggesting that the formation of a disulfide bond at position 2 blocked ionic currents. Notably, the current decay induced by $TbHO_2$ was accelerated as Ca^{2+} concentrations were increased suggesting the likelihood of disulfide linking between cysteines occurs more readily when channels are in a physiological closed conformation (Fig. 4 *B* and *C*). Disulfide bridge formation was further confirmed via connexin dimer generation in nonreducing western blot analysis (*SI Appendix*, Fig. S8). In addition, we evaluated whether formation of metal bridges with Cd^{2+} (100 nM) mimics the effect observed with $TbHO_2$. As expected, the exponential current decay by Cd^{2+} blockade was also accelerated in a Ca^{2+}-dependent manner (Fig. 4*D*). Taken together, these data suggest that the NTs (where +2C was introduced) come in close proximity when hemichannels transition with higher occupancy to the closed state induced by extracellular Ca^{2+}.

Next, we applied the same strategy to determine whether molecule permeation is affected by the crosslinking between cysteines in the NT. In control conditions, hemichannels formed by Cx26B +2C were permeable to DAPI, as observed in WT hemichannels. However, upon treatment with 2 mM $TBHO_2$, DAPI permeation was completely abolished in Cx26B +2C hemichannels but not in the control Cx26B hemichannels (Fig. 4 *E* and *F*). This finding indicates that atomic ions and molecules are transported through the pore and that NT rearrangements are necessary for both ionic and molecule permeation.

Transport of Molecules Occurs Independently of Ionic Conduction. Previous studies reported high permeability rates for fluorescent dyes at negative membrane potentials, while ionic currents remain undetected (14, 18). These findings contradict the concept that a channel with an intrinsically wide permeation pathway will permit free diffusion for both ions and molecules. Taking advantage of the TEVC/dye uptake assay, we assessed whether molecule permeation correlates with the increase of ionic flux in a voltage-dependent manner. DAPI uptake in oocytes expressing Cx26 was detected when membrane potential was held at negative membrane potentials (Fig. 5*A*). Strikingly, DAPI uptake was abolished at positive membrane potentials at which the ionic conductance was robust (Fig. 5*A*). The voltage dependence of DAPI transport displayed a Boltzmann relationship inverse to the relative open probability for ionic currents (Fig. 5*B*). This finding strongly indicates that DAPI and atomic ions are not moving simultaneously within the pore.

If the flux of molecules and ions occurs simultaneously within the same conduction pathway, it would be expected that molecules within the pore should reduce the atomic ion flux. Thus, we tested whether macroscopic currents detected by TEVC in oocytes

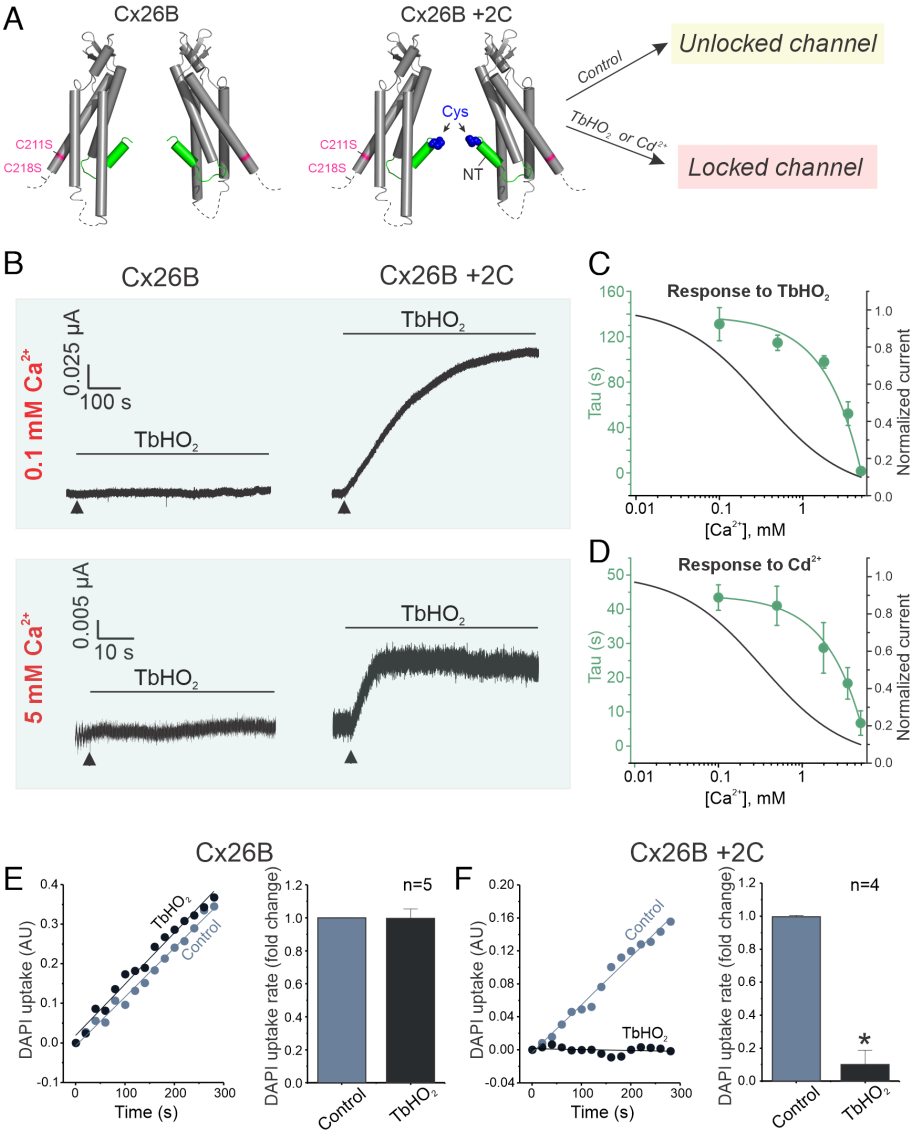

Fig. 4. Molecules require NT rearrangements for translocation through the Cx26 hemichannel. (*A*) Scheme of mutants used for the crosslinking approach. For clarity, only two connexin monomers are shown. In the mutant Cx26B +2C, one cysteine (in blue) was inserted at position 2 in the NT domain, shown in green. Additionally, residues C211 and C218 (in magenta) were replaced with serine to prevent cross-linking at those locations. Met1 is not shown for clarity. Hemichannels formed by C211S and C218S without the cysteine at position 2 (named Cx26B) were used as controls. In theory, only Cx26B +2C channel pore can be locked by the formation of disulfide bridges, when the cysteines are exposed to oxidant agents, such as $TbHO_2$ or by formation of metal bridges, when cysteines are exposed to Cd^{2+}. (*B*) Representative traces of ionic current recorded in oocytes expressing Cx26B or Cx26B +2C. Oocytes were superfused with Ringer solution containing specific Ca^{2+} concentrations, and membrane potential was held at −40 mV. After ionic current stabilization, oocytes were superfused with 2 mM $TbHO_2$ to lock the channels by crosslinking. Arrows indicate the time $TbHO_2$ superfusion starts, and horizontal lines indicate the period of $TbHO_2$ superfusion. (*C*) Analysis of the kinetics of disulfide-bridge formation by calculation of tau values after $TbHO_2$ superfusion. (*D*) Analysis of the kinetics of metal-bridge formation by calculation of Tau values after superfusion with 100 nM Cd^{2+}, following the same experimental approach shown in B-C. Note that channel closure by $TbHO_2$ or Cd^{2+} is faster when the relative open probability is low, and vice versa. (*E*) Representative time courses of DAPI uptake in an oocyte expressing Cx26B (control) before and after incubation with 2 mM $TbHO_2$. For quantification, the DAPI uptake rate was normalized to the control group. (*F*) Representative time courses and quantification of DAPI uptake in oocytes expressing Cx26B +2C before and after incubation with 2 mM $TbHO_2$. For *E* and *F*, DAPI uptake was evaluated in oocytes held at −40 mV. *$P < 0.05$ vs. control by paired Student's *t*-test. Error bars are SEM.

expressing Cx26 are affected by the presence of 200 µM DAPI in the extracellular bath, a saturating concentration for molecule transport as shown in Fig. 1 *C* and *D*. We observed that DAPI did not affect the macroscopic ionic currents in Cx26 hemichannels (Fig. 6*A*). Consistently, single-channel conductance was not affected by the presence of DAPI in the pipette (Fig. 6 *B* and *C*).

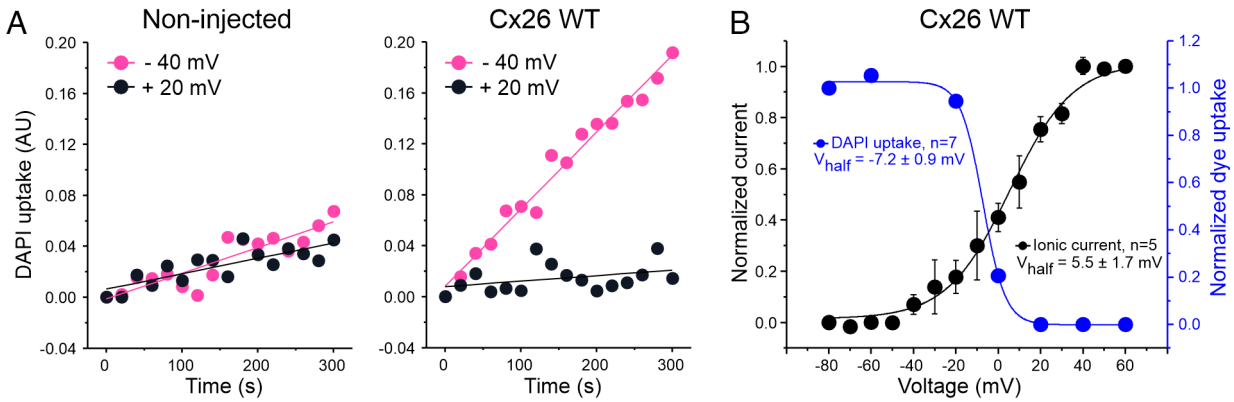

Fig. 5. The transport of molecules in connexin hemichannels is voltage-dependent and favored at physiological negative membrane potentials. (*A*) Representative time courses of the DAPI uptake evaluated in noninjected oocytes (*Left*) or oocytes expressing Cx26 WT (*Right*). Oocytes were superfused with Ringer solution containing 1 mM Ca^{2+} plus 50 µM DAPI dilactate and membrane potential was clamped at −40 mV (magenta). After 5 min recording, membrane voltage was switched to +20 mV (black) and DAPI uptake was recorded again. (*B*) Effect of membrane potential on ionic current (black) and DAPI permeation rate (blue) through Cx26 hemichannels. The voltage dependency for ionic currents was determined by plotting the normalized tail currents recorded after depolarizing pulses (40 s) in the presence of 1 mM Ca^{2+}. Voltage-dependence curves for ionic current and dye uptake were fit with Boltzmann equations (*Materials and Methods*). The Boltzmann parameters for dye uptake were V_{half} = −7.2 ± 0.9 mV; z = 5.17 ± 0.57. The Boltzmann parameters for ionic currents were V_{half} = 5.5 ± 1.7 mV; z = 1.70 ± 0.11. Error bars are SEM.

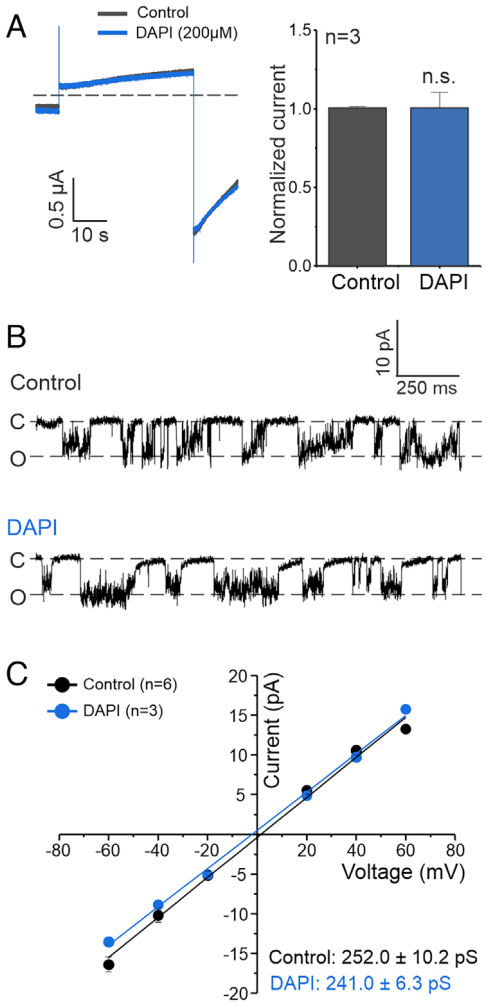

Fig. 6. Permeant molecules do not affect macroscopic ionic currents or single-channel conductance of Cx26 hemichannels. (*A*) Representative ionic current traces recorded by TEVC in oocytes expressing Cx26 WT. Opening of Cx26 hemichannels was induced by a 40 s depolarizing pulse (*Materials and Methods*). A saturating concentration (200 μM) of DAPI was added to the extracellular bath to determine the effect of this permeant on atomic ion permeation. The quantification of the magnitude of tail currents is shown in the bar graph. Values were normalized to the control group. (*B*) Representative single-channel traces recorded in the cell-attached configuration in oocytes expressing Cx26. Dashed lines show the closed (C) and open state (O). (*C*) Quantification of current-voltage relationship from single-channel recordings. Single-channel conductance for each group is shown. n.s.= nonsignificant vs. control by paired Student's *t*-test. Error bars are SEM.

Similarly, a saturating concentration of ethidium did not reduce ionic currents mediated by Cx26 (*SI Appendix*, Fig. S9). These findings indicate that molecules, while using the same pore as atomic ions, do not use it simultaneously, suggesting a different mechanism of permeation.

To unequivocally confirm that molecules can translocate independently of atomic ion flux and building on the striking findings previously mentioned for the $Cx26^{W3A}$ mutant (*SI Appendix*, Fig. S3), we revisited two human NT mutations that previously were shown to lack ionic currents (i.e., loss-of-function mutations): $Cx26^{N14Y}$ and $Cx26^{S17F}$ (25, 26). First, we confirmed by TEVC that these mutations render Cx26 hemichannels "silent" for ion fluxes (Fig. 7 *A*–*C* and *SI Appendix*, Fig. S10 *A* and *B*) and that their expression levels at the plasma membrane were unaffected by the mutations (*SI Appendix*, Fig. S10 *C* and *D*). Then, we tested whether these silent hemichannels could transport molecules. Notably, we observed both mutant channels retained the capability to transport DAPI when expressed in *Xenopus* oocytes or HeLa cells (Fig. 7 *D*–*F* and *SI Appendix*, Fig. S11). Furthermore, these channels were also permeable to ethidium (*SI Appendix*, Fig. S12). Thus, these mutations at the NT block ionic conductance but permit the WT permeability to DAPI and impart permeability to ethidium. Altogether, these data suggest that human mutations that blunt ionic currents do not necessarily affect transport of molecules, supporting that these processes are uncoupled.

To test whether this observation is not restricted to Cx26 hemichannels, we repeated the same approach with Cx30. The T5M mutation abolished the ionic currents (Fig. 7*G*). As observed with Cx26 mutants, hemichannels formed by $Cx30^{T5M}$ were permeable to fluorescent dyes (ethidium in this case) like the WT hemichannel (Fig. 7 *H* and *I*). Dye uptake in both WT and $Cx30^{T5M}$-expressing oocytes was sensitive to La^{3+}, a connexin hemichannel blocker (*SI Appendix*, Fig. S13). We observed a slight reduction in the distribution of $Cx30^{T5M}$ at the plasma membrane and a decrease in the total protein (*SI Appendix*, Fig. S14), which correlated with a lower Vmax for ethidium flux (Fig. 7*J*). This finding suggests that the magnitude of the transport was reduced in oocytes expressing $Cx30^{T5M}$, likely due to the reduction in the number of hemichannels at the plasma membrane. Notably, the Km value for ethidium transport in $Cx30^{T5M}$ was identical to that from WT Cx30 hemichannels, indicating that the kinetic properties for molecular transport were unaffected by the T5M mutation (Fig. 7*J*). These data demonstrate that molecules are transported independently of atomic ion fluxes in at least two different connexin isoforms.

Discussion

A general assumption about the permeation of molecules through large-pore channels is that molecule flux occurs by passive diffusion through the pore, along with the diffusing atomic ions, and that small molecules are discriminated mainly based on the limiting pore width and intrapore charge density when the channel is in the open state. Here, we explored the biophysical properties of the transport of cationic fluorescent dyes through connexin hemichannels to gain fundamental insights regarding the mechanisms that underlay molecule permeation in large-pore channels. While previous studies have shown that different connexin channels can have different molecular selectivity not readily explainable on the basis of size or charge (19, 27, 28), our findings point to the role of specific residues, primarily in the NT domain, that interact with permeants to impart a high degree of selectivity among molecules of similar size and charge. Further, we show that molecular transport throughout these channels is saturable in the micromolar range and displays competitive inhibition. These features are controlled by identified interactions within the pore, particularly with the NT domain. Most importantly, our findings are inconsistent with the current view that permeation of ions and molecules through large-pore channels occurs by the same mechanism. We provide evidence that permeation of molecules and atomic ions can be uncoupled from each other and likely rely on different conformational states and/or dynamics.

Permeation of Molecules through Connexin Hemichannels: Saturability, Binding, and Competition. Our data demonstrate that transport of molecules through Cx26 and Cx30 is saturable and at surprisingly low concentrations, which is consistent with a facilitated diffusion mechanism. Saturability may be shared by other channels forming a wide pore; saturation of cationic fluorescent dye transport has also been found for Cx43 hemichannels and CALHM-1 channels (19, 29, 30). Saturability is not specific to cationic molecules since the flux of cAMP, a negatively charged

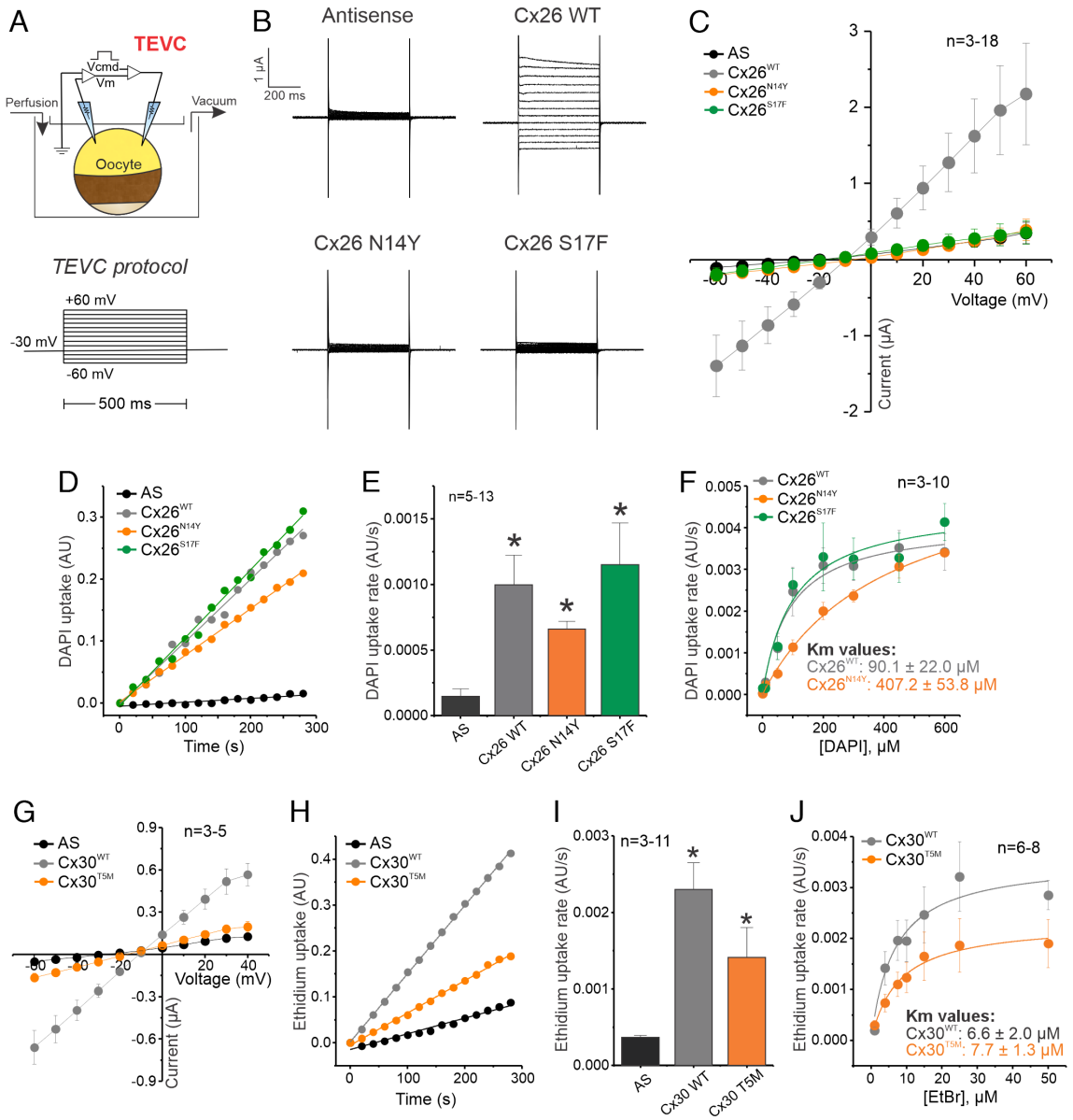

Fig. 7. Pathologic human mutations in connexin hemichannels that lose atomic ion permeability retain the ability to transport small molecules. (*A*) Preparation scheme and TEVC protocol for experiments shown in *B* and *C*. TEVC experiments were performed at low Ca^{2+} concentration (0.2 mM Ca^{2+}) to increase the relative open probability of connexin hemichannels. Voltage pulses were short (500 ms) to assess activation by low extracellular Ca^{2+} rather than voltage. (*B*) Representative traces of the ionic current observed in control oocytes injected with an antisense oligonucleotide (AS) or in oocytes expressing WT or mutant Cx26. (*C*) I–V relationship from data shown in *B*. (*D*) Representative time courses of DAPI uptake in oocytes expressing Cx26 mutants incubated with 50 μM DAPI dilactate. (*E*) Quantification of DAPI uptake rates from data shown in *D*. (*F*) Effect of N14Y and S17F mutations on DAPI permeation kinetics. (*G*) I–V relationship obtained from TEVC experiments performed in oocytes expressing Cx30 or the mutant $Cx30^{T5M}$, using the approach shown in panel *A*. (*H*) Representative time courses of ethidium uptake in oocytes expressing $Cx30^{T5M}$ incubated with 50 μM ethidium bromide (EtBr). (*I*) Quantification of data shown in *H*. (*J*) Effect of T5M mutation on ethidium permeation kinetics. Dye uptake was evaluated at resting membrane potentials. **P* < 0.05 vs. AS, by one-way ANOVA plus Newman–Keuls post hoc test. Error bars are SEM.

endogenous permeant, is also saturable (*SI Appendix*, Fig. S15). Importantly, saturation for all tested molecules occurs in the micromolar range, indicating that saturation of molecule transport does not occur due to the crowding of molecules within the pore. Notably, the Km values calculated for molecule transport in connexin hemichannels are considerably lower than the Km reported for some GLUT transporters, where a millimolar concentration is needed to saturate the facilitated diffusion process (31, 32).

It has been suggested that the molecular selectivity of GJCs and hemichannels arises from binding sites within the pore (27, 33). Recent computational studies of cAMP permeation through Cx26 hemichannels suggested that the pore contains discrete binding sites that interact with cAMP (22). These findings predict saturability of molecular permeation, as we have now demonstrated. Indeed, the occupancy probabilities for DAPI and ethidium along the pore (Figs. 2*A* and 3*A*) suggest that both fluorescent dyes establish favorable interactions with residues at both the NT region and at the extracellular entrance of the pore (where the Ca^{2+} binding region is located). This is consistent with studies showing that these two regions are critical for molecular selectivity (16, 19).

The strongest interaction observed in the MD simulations was a pi–pi stacking between ethidium and residue Trp3 at the NT of Cx26, which hampered in silico permeability to ethidium. We experimentally demonstrated that the ethidium impermeability

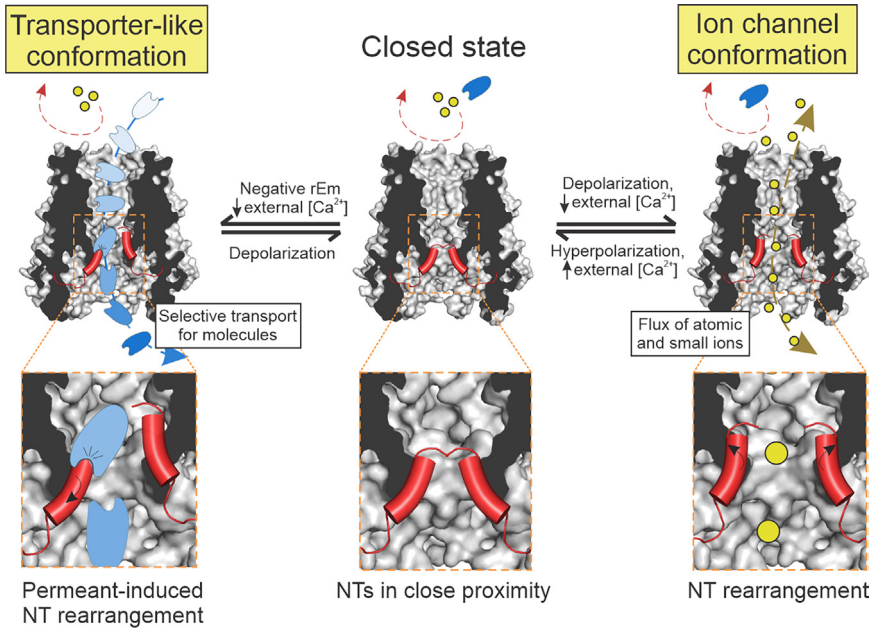

Fig. 8. A proposed mechanism for the independent dual function of connexin hemichannels like molecule transporters or ion channels. In the closed state, hemichannels are not permeable to either atomic ions or small molecules. At negative membrane potentials, a transporter-like conformation is favored, in which the interaction between permeants and specific residues lining the pore finely tunes permeation properties, including transport kinetics and selectivity. We hypothesize that the interaction between permeants and the NT domain (shown in red) triggers a fast and short-term NT rearrangement that allows molecule translocation with no or negligible atomic ion leak. This mechanism is not necessarily disabled by physiological extracellular Ca^{2+} concentrations at which ionic conductance is negligible. Depolarization of the plasma membrane promotes the transition from a state nonconductive to ions to an open state that allows flux of atomic ions (e.g., K^+, Na^+, Ca^{2+}, Cl^-, represented as yellow circles) but not necessarily permeation of molecules (represented in light blue). A low external Ca^{2+} concentration may differentially favor the transition to either the transporter-like state or the ion channel state. Under these conditions, ions can passively move through the pore following their electrochemical gradient, likely because of an allosteric coupling between the Ca^{2+}-binding site in the extracellular region and the NT domain that keeps the gate open.

in Cx26 hemichannels likely resulted from this interaction because 1) W3A mutation or insertion of an alanine at position 3 (Cx26 +3A) to disrupt this pi–pi stacking interaction enabled ethidium transport; 2) ethidium acts as a competitive inhibitor for DAPI permeation, which indicates that ethidium has access to the inner pore, as predicted by MD simulations even though not permeable. This is also consistent with the findings from MD simulations and mutagenesis experiments showing that DAPI interacts with the NT domain, specifically with Asp2, in practically the same region as ethidium.

Importantly, the NT domain in connexin channels defines the narrowest and most flexible part of the pore as previously shown by cryo-EM, MD simulations, and functional studies (6–11, 19, 22, 34, 35). In our MD simulations, including the one reported previously for cAMP, permeants rotate in response to the local charge and geometry of the pore as they are moving through (22). In particular, the NT serves as a common domain for molecule recognition through a combination of electrostatic and hydrophobic interactions, as well as the entropic effects associated with the different orientations and conformations of the molecule. Hence, it is not surprising that mutations in the NT region often have a significant impact on molecule selectivity and permeation kinetics, as demonstrated by the shift in the apparent affinity when we mutated these sites. For example, ethidium uptake was enabled with different mutations in the NT of Cx26, particularly Cx26 +3A (Fig. 2), W3A (*SI Appendix*, Fig. S3), N14Y, S17F (*SI Appendix*, Fig. S12), and N14K (19).

Cx26 and Cx30 are closely related isoforms sharing ~85% sequence identity, but they display different selectivity to DAPI and ethidium. The NT domain, as well as extracellular residues associated with DAPI and ethidium interaction, are highly conserved in both isoforms, including Trp3, which hampers permeability to ethidium (36). Our data from the Cx26 +3A mutant (in which Trp3 is preserved and alanine is incorporated next to Trp3) demonstrate that the presence of Trp3 is not required to prevent ethidium permeation. Therefore, we hypothesize that the side chain orientation of Trp3 plays a critical role in the impermeability of ethidium. Interestingly, we observed in Cx26 hemichannels that Asp2 in the NT interacts with Lys41 in the TM1 by salt bridges. This specific interaction keeps the NT upright, allowing ethidium to align vertically and form pi–pi interactions with Trp3. Importantly, this salt bridge is absent in Cx30 since Lys41 is replaced by Gln41, therefore affecting NT rearrangement and their side chain orientations. The molecular basis for DAPI impermeability in Cx30 is still unclear. Based on in silico approaches, the Cx30 pore profile could differ from that of Cx26 (19); thus, the pore profile and the associated orientation of specific side chains presumably account for differences in permeability and transport properties. Consistently, different connexin isoforms are known to have different molecular permeabilities, despite substantial overall sequence identity and homology (5, 27, 37).

Uncoupling of Molecule Transport and Atomic Ion Flux. More than 20 y ago, Contreras et al., showed that permeation of molecules can occur at resting membrane potentials in Cx43 hemichannels, but atomic ion fluxes were undetectable under the same conditions (14). This anomaly in ionic and molecule permeation has also been described for other connexins, CALHM-1 and pannexin-1 channels (15, 16, 19). A proposed explanation was that molecule permeation occurred during brief and experimentally unresolved opening of the channels (14). In this study, we demonstrated that molecules can permeate in the absence of ionic conductance, suggesting that molecules and atomic ions are transported by different channel

conformations or dynamics. Consistent with this notion, DAPI did not affect macroscopic or unitary ionic currents of Cx26 hemichannels as would be expected for molecules that occlude or bind within the pore at the same time that ions are diffusing through, as it has been shown using nanopores (38, 39). In a clear demonstration of the disconnect between ion and molecular permeability, we showed that pathological human mutations in the NT domain, which were cataloged as loss-of-function mutants due to the absence of ionic currents, still retained the capability to transport molecules with similar kinetic parameters to those observed for WT channels. These findings indicate that molecules and ion permeation can be uncoupled.

The notion that ion and molecule permeation can be uncoupled is further supported by our finding that DAPI transport through Cx26 hemichannels is enabled at negative membrane potentials, but not at positive potentials, where the ion fluxes are substantial (Fig. 5*B*). This is consistent with a previous report showing that permeation at positive potentials is restricted to ions in Cx46 hemichannels (40). The differential voltage regulation of atomic ion permeation and molecule transport could be explained by hemichannels operating in two modes: a molecule-restricted transport mode at negative potentials and a classical ion channel mode at positive voltages (see the proposed model in Fig. 8).

While our data suggest that connexin hemichannels can favor permeation of either ions or molecules, we cannot rule out that, under specific conditions, a full open state can still mediate permeation of both at the same time, as is assumed for wide pores with large ionic conductance. In this work, we provide evidence that a transition to this expected functionality is not necessarily induced by voltage or low extracellular Ca^{2+}. First, the fact that positive potentials abolish DAPI permeation suggests that voltage-induced activation allows the transition to an open state that is permeable to ions but not molecules as previously suggested (40). Second, we found that in the presence of 1 mM extracellular Ca^{2+} Cx26 hemichannel currents were reduced by ~95%, but under the same conditions, molecule permeation was reduced by only 50%, without effect on Km (*SI Appendix*, Fig. S16). Interestingly, a similar effect was recently observed in CALHM1 channels using a different cationic dye, YO-PRO-1 (19). Consistent with this, ionic conductance and ethidium transport are differentially affected by extracellular Ca^{2+} or Mg^{2+} in Cx30 hemichannels (41). Altogether, these data indicate that the magnitude of molecule transport does not correlate with the channel open probability reported by ionic conductance. We view it more likely that low Ca^{2+} can favor two states with preferential permeation to ions or to molecules but not to both simultaneously through the same pore configuration. Based on our findings, we hypothesize that extracellular Ca^{2+} might serve as a physiological modulator to maintain hemichannels closed to atomic ions preventing changes in resting membrane potential or the loss of electrochemical gradient, without disabling the mechanism for molecule transport.

The NT Domain Is a Flexible Domain with Critical Roles in Gating and Molecule Translocation. Structural studies have shown that the NT domain of Cx26 and Cx46/50 is folded into the pore, often parallel to the transmembrane segments, against the pore wall, as for other large-pore channels including innexin, pannexin, CALHM, and LRRC8 channels (6, 7, 42–48). However cryo-EM structures of Cx31.3 and Cx43 also show the NT domain separated from the pore wall and lying parallel to the axis of the plasma membrane, thereby narrowing the pore (9, 10). These and other data suggest that the NT of connexin hemichannels is a flexible intrapore domain, and therefore might serve as a gate for permeants (49). Here, by using extracellular Ca^{2+} as a connexin gating modulator, we experimentally demonstrated rearrangements of the NT domain in a state-dependent manner. The NTs of adjacent subunits come into proximity when the channel is closed by extracellular Ca^{2+}. Notably, Ca^{2+} binding sites are localized in the extracellular part of the pore (24, 50); this also implies that there is an allosteric coupling between the Ca^{2+} sensing domain at the extracellular side and the NT at the intracellular side of the pore.

We propose here that movements of individual NTs are necessary to translocate small molecules across the pore with negligible fluxes of atomic ions. We support this notion with MD simulations showing that molecules directly interact with one or two NTs, triggering fast and short-term rearrangements. Experimental data support these interactions, showing that immobilization of the NT domains via disulfide bridges prevents molecule transport. Importantly, individual NT rearrangement has been already observed in structural studies for Cx43 (11).

Further studies must be carried out to elucidate how a large-pore channel may transport molecules with an undetectable flux of atomic ions. Based on our data, we hypothesize that the dynamics of the pore with a permeant present and the proper interaction between the permeant with the NT domain in a closed state can trigger a fast and short-term movement of the NT domain that adjusts to the closed state immediately after the permeant leaves the NT region (i.e., a facilitated diffusion-like mechanism in which interaction of molecules with the NT induce their own translocation). Alternatively, a second gate/barrier specific for atomic ions could be present in our predicted conformation that allows molecule but not ion permeation. Either scenario would satisfy the minimal requirement for a transporter-like process, in which substrate binding induces a conformational change that shifts the barrier to substrate movement from one side of the substrate to the other (51).

The findings from this work have critical implications for the physiological and pathological role of connexin hemichannels. For instance, electrostatic and hydrophobic interactions with the NT are likely the major determinants of selectivity and permeation kinetics for molecules that fit within the pore. Second, permeation of molecules can be uncoupled from atomic ion flux and rely on a "transporter-like" state impermeable to atomic ions. This state is favored at negative resting potentials and not disabled at physiological millimolar Ca^{2+} concentrations, in which connexin-dependent atomic ion flux is almost negligible. Connexin hemichannels might have distinguishable roles as ion channels and molecule transporters in health and disease. This implies that the mechanisms by which connexin human mutations produce diseases, specifically regarding molecular signaling through hemichannels and perhaps GJCs, should be reevaluated.

Materials and Methods

Molecular Biology and Connexin Expression. Human Cx26 and Cx30 cDNAs were synthesized and subcloned into vectors for expression in *Xenopus* oocytes and HeLa cells. Mutations were introduced using site-directed mutagenesis. *Xenopus* oocytes were microinjected with connexin cRNAs and antisense oligonucleotides to reduce the expression of the endogenous Cx38. Details on molecular biology, oocyte collection, and oocyte microinjection can be found in *SI Appendix, Supplementary Materials and Methods*.

Molecule Permeability Assays. Dye uptake experiments were performed in oocytes using the TEVC/Dye uptake technique, as recently described (19, 20). cAMP measurement assays were conducted in oocytes by an ELISA. Additional dye uptake assays were conducted in transfected HeLa cells using a multimode plate reader. Details on oocyte preparation for fluorescence-based dye uptake assays, TEVC/Dye uptake technique, determination of kinetic parameters of molecule permeation, cAMP measurements, and dye uptake assays in HeLa cells are described in *SI Appendix, Supplementary Materials and Methods*.

Electrophysiology. TEVC experiments were performed as previously described (19, 24). Single-channel recordings of connexin hemichannels in *Xenopus* oocytes were performed by patch clamp (cell-attached configuration) as described previously (52, 53). Detailed protocols, solutions, and methods related to electrophysiological recordings can be found in *SI Appendix, Supplementary Materials and Methods*.

Molecular Dynamics (MD). Simulations were conducted using established atomic models of Cx26 hemichannels embedded within lipid bilayers as previously described (22, 23). Details on MD simulations (Atomistic model preparation, force fields, equilibrium/production protocols, and voltage simulations) are included in *SI Appendix, Supplementary Materials and Methods*.

Statistical analysis was performed using appropriate tests, with significance set at $P < 0.05$. Further details regarding the reagents and methods used in this study are available in *SI Appendix, Supplementary Materials and Methods*.

Data, Materials, and Software Availability. All study data are included in the article and/or *SI Appendix*.

ACKNOWLEDGMENTS. This work was supported by the NIH/National Institute of General Medical Sciences (Grants R01-GM099490 to J.E.C., and R01-GM101950 to A.L.H. and J.E.C.). Computational resources were provided via the Extreme Science and Engineering Discovery Environment allocation TG-MCB160119, which is supported by NSF Grant No. ACI-154862.

Author affiliations: [a]Department of Physiology and Membrane Biology, School of Medicine, University of California, Davis, CA 95616; [b]Department of Biotechnology and Pharmaceutical Sciences, College of Pharmacy, Western University of Health Sciences, Pomona, CA 91766; and [c]Department of Pharmacology, Physiology, and Neuroscience, New Jersey Medical School, Rutgers, The State University of New Jersey, Newark, NJ 07103

1. D. Zhao *et al.*, Connexin hemichannels with prostaglandin release in anabolic function of bone to mechanical loading. *eLife* **11**, e74365 (2022).
2. L. M. Tovar *et al.*, Understanding the role of ATP release through connexins hemichannels during neurulation. *Int. J. Mol. Sci.* **24**, 2159 (2023).
3. J. C. Sáez *et al.*, Cell membrane permeabilization via connexin hemichannels in living and dying cells. *Exp. Cell Res.* **316**, 2377–2389 (2010).
4. D. A. Goodenough, D. L. Paul, Beyond the gap: Functions of unpaired connexon channels. *Nat. Rev. Mol. Cell Biol.* **4**, 285–295 (2003).
5. A. L. Harris, Connexin channel permeability to cytoplasmic molecules. *Progr. Biophys. Mol. Biol.* **94**, 120–143 (2007).
6. S. Maeda *et al.*, Structure of the connexin 26 gap junction channel at 3.5 Å resolution. *Nature* **458**, 597–602 (2009).
7. J. B. Myers *et al.*, Structure of native lens connexin 46/50 intercellular channels by cryo-EM. *Nature* **564**, 372–377 (2018).
8. J. A. Flores *et al.*, Connexin-46/50 in a dynamic lipid environment resolved by CryoEM at 1.9 Å. *Nat. Commun.* **11**, 4331 (2020).
9. H.-J. Lee *et al.*, Cryo-EM structure of human Cx31.3/GJC3 connexin hemichannel. *Sci. Adv.* **6**, eaba4996 (2020).
10. C. Qi *et al.*, Structure of the connexin-43 gap junction channel in a putative closed state. *eLife* **12**, RP87616 (2023).
11. H.-J. Lee *et al.*, Conformational changes in the human Cx43/GJA1 gap junction channel visualized using cryo-EM. *Nat. Commun.* **14**, 931 (2023).
12. V. Verselis, R. L. White, D. C. Spray, M. V. L. Bennett, Gap junctional conductance and permeability are linearly related. *Science* **234**, 461–464 (1986).
13. G. Kanaporis, P. R. Brink, V. Valiunas, Gap junction permeability: Selectivity for anionic and cationic probes. *Am. J. Physiol. Cell Physiol.* **300**, C600–C609 (2011).
14. J. E. Contreras, J. C. Sáez, F. F. Bukauskas, M. V. L. Bennett, Gating and regulation of connexin 43 (Cx43) hemichannels. *Proc. Natl. Acad. Sci. U.S.A.* **100**, 11388–11393 (2003).
15. B. S. Nielsen *et al.*, Pannexin 1 activation and inhibition is permeant-selective. *J. Physiol.* **598**, 361–379 (2020).
16. B. S. Nielsen *et al.*, Structural determinants underlying permeant discrimination of the Cx43 hemichannel. *J. Biol. Chem.* **294**, 16789–16803 (2019).
17. D. B. Hansen, T. H. Braunstein, M. S. Nielsen, N. MacAulay, Distinct permeation profiles of the connexin 30 and 43 hemichannels. *FEBS Lett.* **588**, 1446–1457 (2014).
18. D. B. Hansen *et al.*, Activation, permeability, and inhibition of astrocytic and neuronal large pore (hemi)channels. *J. Biol. Chem.* **289**, 26058–26073 (2014).
19. P. S. Gaete *et al.*, A novel voltage-clamp/dye uptake assay reveals saturable transport of molecules through CALHM1 and connexin channels. *J. Gen. Physiol.* **152**, e202012607 (2020).
20. P. S. Gaete, J. E. Contreras, "Chapter Eleven–A method for assessing ionic and molecular permeation in connexin hemichannels" in *Methods in Enzymology, Ion Channels: Channel Chemical Biology, Engineering, and Physiological Function*, D. L. Minor, H. M. Colecraft, Eds. (Academic Press, 2021), pp. 271–293.
21. T. Kwon, A. L. Harris, A. Rossi, T. A. Bargiello, Molecular dynamics simulations of the Cx26 hemichannel: Evaluation of structural models with Brownian dynamics. *J. Gen. Physiol.* **138**, 475–493 (2011).
22. W. Jiang *et al.*, Free energy and kinetics of cAMP permeation through connexin26 via applied voltage and milestoning. *Biophys. J.* **120**, 2969–2983 (2021).
23. Y. Luo, A. R. Rossi, A. L. Harris, Computational studies of molecular permeation through Connexin26 channels. *Biophys. J.* **110**, 584–599 (2016).
24. W. Lopez *et al.*, Mechanism of gating by calcium in connexin hemichannels. *Proc. Natl. Acad. Sci. U.S.A.* **113**, E7986–E7995 (2016).
25. J. R. Lee, A. M. DeRosa, T. W. White, Connexin mutations causing skin disease and deafness increase hemichannel activity and cell death when expressed in *Xenopus* oocytes. *J. Invest. Dermatol.* **129**, 870–878 (2009).
26. H. A. Sanchez, N. Slavi, M. Srinivas, V. K. Verselis, Syndromic deafness mutations at Asn 14 differentially alter the open stability of Cx26 hemichannels. *J. Gen. Physiol.* **148**, 25–42 (2016).
27. C. G. Bevans, M. Kordel, S. K. Rhee, A. L. Harris, Isoform composition of connexin channels determines selectivity among second messengers and uncharged molecules. *J. Biol. Chem.* **273**, 2808–2816 (1998).
28. E. B. Trexler, F. F. Bukauskas, J. Kronengold, T. A. Bargiello, V. K. Verselis, The first extracellular loop domain is a major determinant of charge selectivity in Connexin46 channels. *Biophys. J.* **79**, 3036–3051 (2000).
29. J. A. Orellana *et al.*, Cation permeation through connexin 43 hemichannels is cooperative, competitive and saturable with parameters depending on the permeant species. *Biochem. Biophys. Res. Commun.* **409**, 603–609 (2011).
30. J. C. Sáez *et al.*, Permeation of molecules through astroglial Connexin 43 hemichannels is modulated by cytokines with parameters depending on the permeant species. *Int. J. Mol. Sci.* **21**, 3970 (2020).
31. M. Mueckler, B. Thorens, The SLC2 (GLUT) family of membrane transporters. *Mol. Aspects Med.* **34**, 121–138 (2013).
32. A. R. Manolescu, R. Augustin, K. Moley, C. Cheeseman, A highly conserved hydrophobic motif in the exofacial vestibule of fructose transporting SLC2A proteins acts as a critical determinant of their substrate selectivity. *Mol. Membr. Biol.* **24**, 455–463 (2007).
33. P. A. Weber, H.-C. Chang, K. E. Spaeth, J. M. Nitsche, B. J. Nicholson, The permeability of gap junction channels to probes of different size is dependent on connexin composition and permeant-pore affinities. *Biophys. J.* **87**, 958–973 (2004).
34. F. Zonta, G. Polles, G. Zanotti, F. Mammano, Permeation pathway of homomeric Connexin 26 and Connexin 30 channels investigated by molecular dynamics. *J. Biomol. Struct. Dyn.* **29**, 985–998 (2012).
35. P. E. M. Purnick, D. C. Benjamin, V. K. Verselis, T. A. Bargiello, T. L. Dowd, Structure of the amino terminus of a gap junction protein. *Arch. Biochem. Biophys.* **381**, 181–190 (2000).
36. D. Bai, Structural analysis of key gap junction domains–Lessons from genome data and disease-linked mutants. *Semin. Cell Dev. Biol.* **50**, 74–82 (2016).
37. R. D. Veenstra, Size and selectivity of gap junction channels formed from different connexins. *J. Bioenerg. Biomembr.* **28**, 327–337 (1996).
38. G. Huang, A. Voet, G. Maglia, FraC nanopores with adjustable diameter identify the mass of opposite-charge peptides with 44 dalton resolution. *Nat. Commun.* **10**, 835 (2019).
39. A. K. Thakur, L. Movileanu, Real-time measurement of protein–protein interactions at single-molecule resolution using a biological nanopore. *Nat. Biotechnol.* **37**, 96–101 (2019).
40. Y. Qu, G. Dahl, Function of the voltage gate of gap junction channels: Selective exclusion of molecules. *Proc. Natl. Acad. Sci. U.S.A.* **99**, 697–702 (2002).
41. B. S. Nielsen, J. S. Alstrom, B. J. Nicholson, M. S. Nielsen, N. MacAulay, Permeant-specific gating of connexin 30 hemichannels. *J. Biol. Chem.* **292**, 19999–20009 (2017).
42. J. L. Syrjänen, M. Epstein, R. Gómez, H. Furukawa, Structure of human CALHM1 reveals key locations for channel regulation and blockade by ruthenium red. *Nat. Commun.* **14**, 3821 (2023).
43. D. Deneka, M. Sawicka, A. K. M. Lam, C. Paulino, R. Dutzler, Structure of a volume-regulated anion channel of the LRRC8 family. *Nature* **558**, 254–259 (2018).
44. G. Kasuya *et al.*, Cryo-EM structures of the human volume-regulated anion channel LRRC8. *Nat. Struct. Mol. Biol.* **25**, 797–804 (2018).
45. W. Choi, N. Clemente, W. Sun, J. Du, W. Lü, The structures and gating mechanism of human calcium homeostasis modulator 2. *Nature* **576**, 163–167 (2019).
46. K. Demura *et al.*, Cryo-EM structures of calcium homeostasis modulator channels in diverse oligomeric assemblies. *Sci. Adv.* **6**, eaba8105 (2020).
47. K. Michalski *et al.*, The Cryo-EM structure of pannexin 1 reveals unique motifs for ion selection and inhibition. *eLife* **9**, e54670 (2020).
48. J. L. Syrjanen *et al.*, Structure and assembly of calcium homeostasis modulator proteins. *Nat. Struct. Mol. Biol.* **27**, 150–159 (2020).
49. A. K. Khan *et al.*, A steric, "ball-and-chain" mechanism for pH-mediated regulation of gap junction channels. *Cell Rep.* **31**, 107482 (2020).
50. W. Lopez, J. Gonzalez, Y. Liu, A. L. Harris, J. E. Contreras, Insights on the mechanisms of Ca^{2+} regulation of connexin26 hemichannels revealed by human pathogenic mutations (D50N/Y). *J. Gen. Physiol.* **142**, 23–35 (2013).
51. D. Drew, O. Boudker, Shared molecular mechanisms of membrane transporters. *Annu. Rev. Biochem.* **85**, 543–572 (2016).
52. I. E. García *et al.*, The syndromic deafness mutation G12R impairs fast and slow gating in Cx26 hemichannels. *J. Gen. Physiol.* **150**, 697–711 (2018).
53. J. M. Valdez Capuccino *et al.*, The connexin26 human mutation N14K disrupts cytosolic intersubunit interactions and promotes channel opening. *J. Gen. Physiol.* **151**, 328–341 (2018).